JOURNAL OF MATERIALS SCIENCE **36** (2001) 5447–5455

Nano-precipitation in hot-pressed silicon carbide

X. F. ZHANG*, M. E. SIXTA‡, D. CHEN*, L. C. DE JONGHE*,‡
*Materials Sciences Division, Lawrence Berkeley National Laboratory, ‡Department of Materials Science and Mineral Engineering, University of California, Berkeley, CA 94720

Heat treatments at 1300°C, 1400°C, 1500°C, and 1600°C in Ar were found to produce nanoscale precipitates in hot-pressed silicon carbide containing aluminum, boron, and carbon sintering additives (ABC-SiC). The precipitates were studied by transmission electron microscopy (TEM) and nano-probe energy-dispersive X-ray spectroscopy (nEDS). The precipitates were plate-like in shape, with a thickness, length and separation of only a few nanometers, and their size coarsened with increasing annealing temperature, accompanied by reduced number density. The distribution of the precipitates was uniform inside the SiC grains, but depleted zones were observed in the vicinity of the SiC grain boundaries. A coherent orientation relationship between the precipitates and the SiC matrix was found. Combined high-resolution electron microscopy, computer simulation, and nEDS identified an Al_4C_3-based structure and composition for the nano-precipitates. Most Al ions in SiC lattice exsolved as precipitates during the annealing at 1400 to 1500°C. Formation mechanism and possible influences of the nanoscale precipitates on mechanical properties are discussed.

1. Introduction

High performance structural ceramics, both at ambient and at high temperatures, require a combination of many mechanical properties including strength, creep resistance, toughness, and wear resistance. For monolithic polycrystalline ceramics such as SiC and Si_3N_4, the mechanical properties are known to be determined by microstructure and composition of the grains and grain boundaries [1–13]. In some instances advantageous combinations of several of these properties have been achieved [12]. Grain boundaries formed in as-sintered polycrystalline ceramics often contain amorphous films [6, 10, 14–16], and in a previous paper we reported that suitable post-annealing of ABC-SiC could crystallize the amorphous grain boundaries [16]. Indeed, the heat-treated ABC-SiC samples showed a considerable increase in bend strength, toughness, and creep resistance [12, 13, 17]. Another possible effect of a heat treatment is to produce precipitates, a classic technique to strengthening metals and alloys. While manipulation of precipitation is abundant in metallic systems, in ceramic systems this technique is less common, because mismatch stresses are less readily relieved and may lead to spontaneous crack initiation.

The solubility limit of aluminum and boron in SiC increases with temperature [18], therefore controlled precipitation should be possible in the SiC grains during a suitable post-annealing procedure. This precipitation can be exploited as an additional tool in controlling the properties, such as wear resistance and hardness, of the silicon carbide ceramics. In this paper, we report on nanoscale precipitation induced in ABC-SiC grains by heat treatments.

2. Experimental

3 wt% aluminum, 0.6 wt% boron, and 2 wt% carbon were mixed with submicron β-3C SiC powders (B20, H. C. Starck, Germany). After stir drying, sieving, and cold die compaction, the powders were hot-pressed at 1900°C, for 1 h, in an Ar environment, at 50 MPa, in a graphite die lined with graphite foil. The furnace was then cooled down to room temperature at a rate of 10°C/min. The resulting SiC samples were 99% dense, with dominant α-4H and α-6H SiC phases as identified by X-ray diffraction. Details about the processing conditions and mechanical properties were published previously [8, 9]. TEM characterizations for structure and composition of the grain boundaries [16], and secondary phases [19], were reported earlier. The as-hot-pressed samples were heat treated in a tungsten mesh furnace with flowing Ar, at a temperature of 1300°C for 85 hrs, 1400°C for 840 hrs, 1500 and 1600°C for 168 hrs in Ar.

Both as-hot-pressed and post-annealed ABC-SiC samples were examined by analytical and high-resolution TEM in a field-emission-gun Philips CM200 transmission electron microscope working at 200 kV. The microscope was equipped with an EDS system, which was capable of probing chemical information in areas of nanometer dimensions. In this study, an 8 nm diameter probe was formed for EDS analysis.

3. TEM characterization

The as-hot-pressed polycrystalline samples were consisted of plate-like, elongated SiC grains with lengths and thicknesses ranging from 3 to 11 μm and 1 to 3 μm,

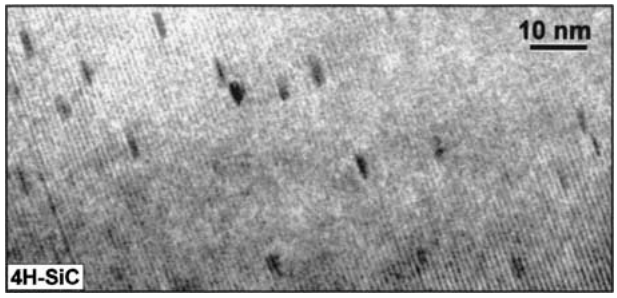

Figure 1 Lattice-fringe image showing nanoscale precipitates in a 4H-SiC grain. The sample was annealed at 1300°C for 85 hrs.

respectively, embedded in smaller and equiaxed SiC grains, forming a bimodal microstructure [19]. Trace amounts of Al were consistently detectable in the SiC grain bulk, together with Al concentrations in the SiC grain boundary films or in secondary phases [16, 19]. After annealing at 1300°C for 85 hrs, highly dense ($\sim 5 \times 10^{22}/m^3$), and very small precipitates were observed inside SiC grains, as shown in a lattice-fringe image in Fig. 1. Most precipitates were about 1 nm thick, 3 to 5 nm long, with a projected minimum separation of about 2 nm.

Compared with precipitates formed in the 1300°C heat treatment, the size of the precipitates was much bigger after a heat treatment at 1400°C. The TEM micrograph in Fig. 2 shows an α-SiC grain close to the [11$\bar{2}$ 0] zone-axis direction, in a sample after annealing at 1400°C for 840 hrs in Ar. The most striking feature of the image, apart from the alternating light and dark bend contours, is the appearance of a high projected density of nanometer-sized precipitates. The nano-precipitates were anisotropic in shape, typically elongated in the (0001) planes of the α-SiC matrix. Most precipitates were 2 to 5 nm thick, 7 to 10 nm long, with a projected minimum separation of about 4 nm. Assuming the width and length of the plate-like precipitates to be the same, the average volume of a precipitate is about 300 nm^3, much larger than that of 1300°C-annealed samples, but their projected number density is reduced by five times to about $1 \times 10^{22}/m^3$.

The plate-like shape indicated a preferred growth direction, parallel to the basal plane of the α-SiC. An intriguing feature is that some precipitates, as indicated by a bold arrow in Fig. 2, were even more highly anisotropic and appeared to be lined up along a particular basal plane. Selected-area electron diffraction did not show extra reflections distinguishable from those of the α-SiC. This was attributed to the extremely small size of the precipitates, while a similarity in structure and a high degree of lattice coherence between the precipitates and the SiC matrix could also be deduced from the general absence of strain-field contrast around the precipitates.

After annealing at 1500°C for 168 hrs, the typical precipitates were again even larger than those in the 1400°C-annealed samples. However, significant

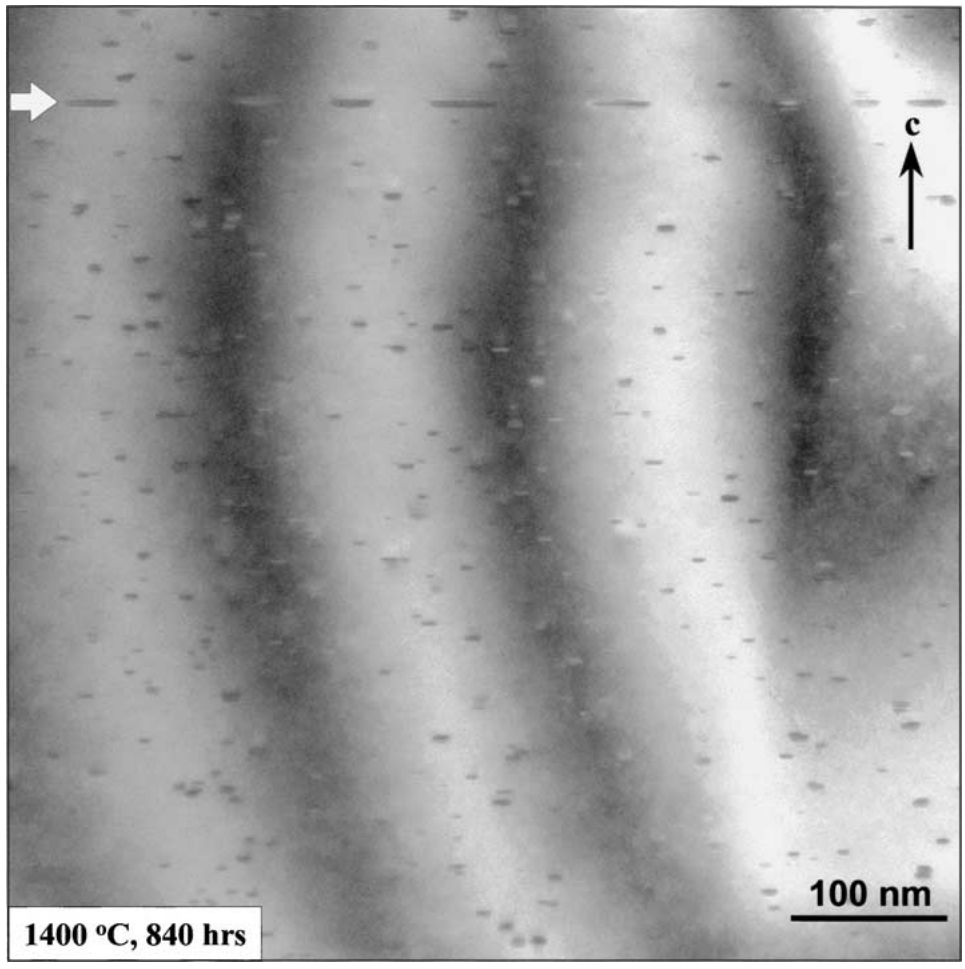

Figure 2 A TEM micrograph showing highly dense nanoscale precipitates in the ABC-SiC annealed at 1400°C for 840 hrs. A bold arrow indicates the unusually elongated precipitates.

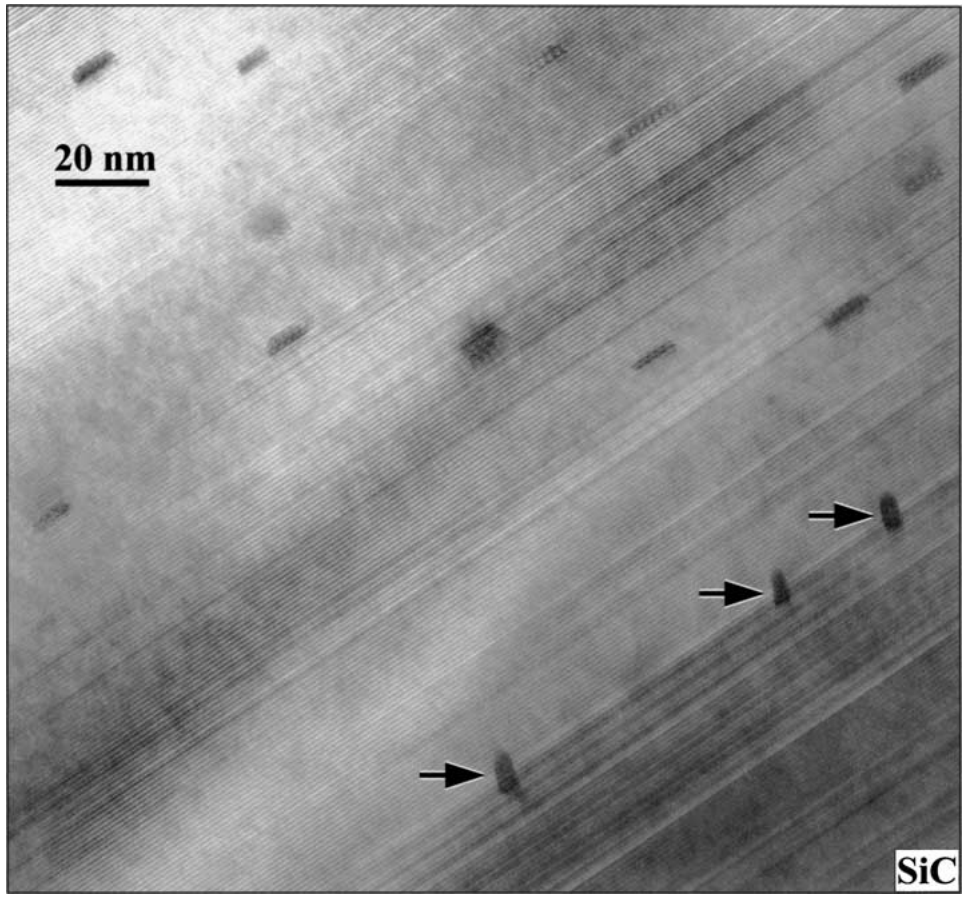

Figure 3 Lattice-fringe image showing precipitates formed in ABC-SiC annealed at 1600°C for 168 hrs. Note the bigger size but less amount density of the precipitates compared with those in Figs 1 and 2. Three precipitates titled away from the SiC (0001) habit plane are indicated by arrows.

coarsening was observed only after annealing at 1600°C (168 hrs), as shown in Fig. 3, in which the precipitates still show a plate-like shape, now typically 9 to 30 nm long and 3 to 8 nm thick, with a projected minimum separation of about 7 nm. The average volume of the precipitates was now about 2200 nm^3, more than 6 times larger than that of the precipitates in 1400°C-annealed samples. In contrast, the projected number density, $2 \times 10^{21}/m^3$, is about ten times lower. The size change with increasing annealing temperatures is summarized in Table I.

In addition to the difference in volumes, change in aspect ratio of the plate-like precipitates can also be noticed from Table I. The aspect ratio was reduced from about 4 in the 1300°C-annealed samples to about 3 in the 1600°C-annealed samples. Obviously, the precipitates tend to grow faster in the habit planes in the initial stage (lower annealing temperature), and grow more 3-dimensionally with increasing annealing temperature. At 1600°C, the precipitates became unstable, some of them moved off the habit plane, as indicated by arrows in Fig. 3.

The volume fraction of the precipitates in SiC grains can be simply calculated as: Volume fraction = Mean volume × Number density, once the foil thickness is known or estimated from the image characteristics. The calculated values are given in Table I. The volume fraction increased by a factor of 3.8 from 1300°C to 1400°C, and remains almost constant till 1600°C. This implied that precipitation was almost completed during

TABLE I Morphology and distribution of the nano-precipitates formed in the annealed ABC-SiC. The 1300–30 h denotes annealing at 1300°C for 30 hrs. Similar meaning is for other notes. The volume of the precipitates was calculated assuming an equivalent length and width

	Annealing conditions (ABC-SiC)			
Nano-precipitates	1300–30 h	1400–840 h	1500–168 h	1600–168 h
Length (nm)	3–5	7–10	9–15	9–30
Thickness (nm)	0.9–1.1	2–5	2–5	3–8
Aspect ratio	3.8–4.2	2.0–4.0	2.0–4.0	2.0–4.0
Separation (nm)	>2	>4	>7	>7
Volume (nm^3)	18	100–700	400–1000	1500–2500
(mean value)	(16)	(300)	(428)	(2200)
Number density ($1/m^3$)	5×10^{22}	1×10^{22}	7×10^{21}	2×10^{21}
Volume fraction[a]	0.8×10^{-3}	3×10^{-3}	3×10^{-3}	4.4×10^{-3}
Depletion zone (nm)	50–80	50–100	120–200	250–300

[a]Volume fraction = Mean volume × Density.

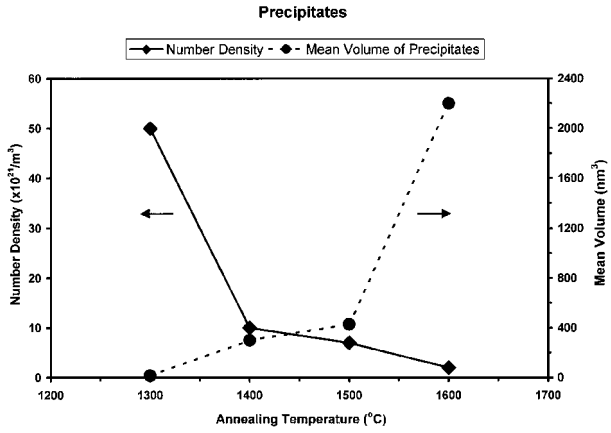

Figure 4 A plot for change of number density and mean volume of the precipitates with increasing annealing temperature.

annealing at 1400 to 1500°C. nEDS analysis confirmed this conclusion as will be seen later. At higher temperature the lattice diffusion merged small precipitates, resulting in larger size but reduced number density. This tendency can be clearly seen in a plot in Fig. 4.

It is interesting to note that no nano-precipitates were found in samples annealed at temperatures at or below 1200°C for even more than 800 hrs. Since it is unlikely that the A1 solubility in SiC should increase at lower temperatures, this lack of precipitation can be attributed to slow diffusion kinetics.

The nanoscale precipitates could be best observed by using TEM when tilting the specimen to a direction perpendicular to the **c**-axis of the α-SiC grain. This feature is demonstrated in Fig. 5, in which high density of nano-precipitates in the projected plane is evident in the SiC grain on the upper-right side of the image, while the existence of the precipitates in the lower-left SiC grain was not obvious because of the unfavorable imaging orientation. Another interesting feature revealed in Fig. 5 is the precipitate-depleted zone, approximately 65 nm wide marked by the two dot lines. Precipitate-depleted zones, about 50–100 nm wide on each side of the grain boundaries, were a common feature in the samples after 1400°C annealing. After 1300°C heat treatment, the precipitate-free zone was about 50–80 nm, increasing to about 120–200 nm, and 250–300 nm, after annealing at 1500°C, and 1600°C for 168 hrs, respectively.

According to Fig. 5, assuming that all Al in the depletion zone is transported to and absorbed by the grain boundary, it is possible to estimate, within an order of magnitude, the Al diffusion coefficient in the SiC lattice at 1400°C. With an average depleted zone width of $\Delta x = 75$ nm after annealing for $t = 840$ hrs, an approximate Al diffusion coefficient in SiC at 1400°C can be estimated: $D_{\mathrm{Al}} \approx (\Delta x)^2/2t \approx 9 \times 10^{-18}$ cm^2/sec. Using the same argument, we obtain $D_{\mathrm{Al}} \approx 1 \times 10^{-16}$ cm^2/sec at 1500°C, and $D_{\mathrm{Al}} \approx 6 \times 10^{-16}$ cm^2/sec at 1600°C.

Because of the nanometer scale of the precipitates, an 8 nm diameter electron beam probe was formed to perform nEDS line-scans across the thickness of the precipitates. The line-scan is shown schematically in Fig. 6a. The beginning and ending scan spots were on the SiC matrix. The dwell time of the electron beam probe on each scan spot was 5 sec. A resultant line-scan profile is shown in Fig. 6b, in which only the change in

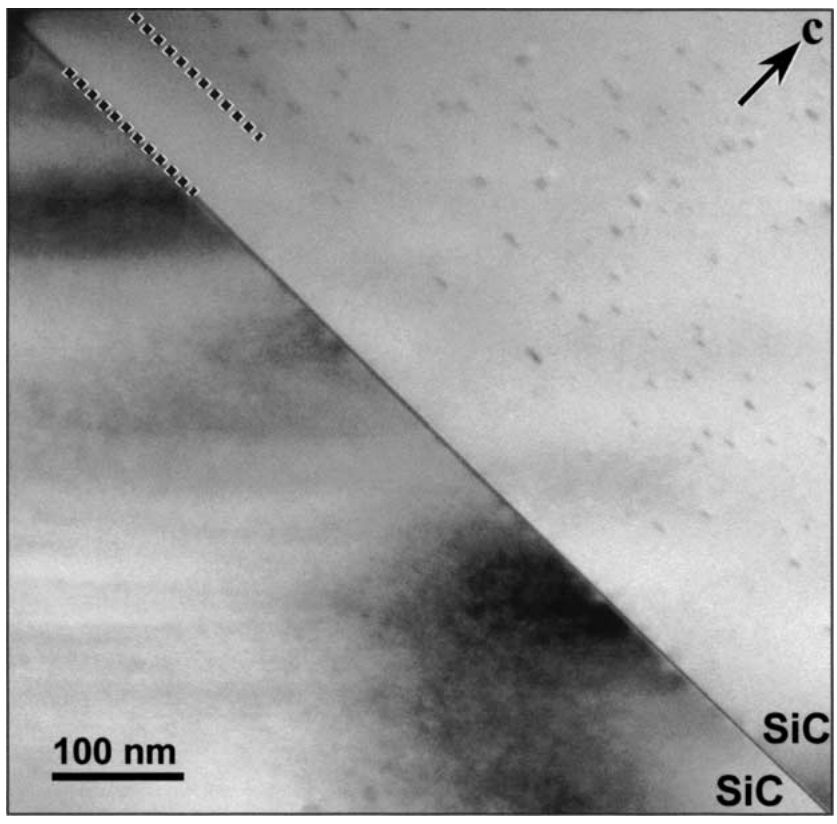

Figure 5 A TEM micrograph showing a SiC grain boundary and the vicinity area in a sample annealed at 1400°C. Nano-precipitates can be seen in the upper-right side SiC grain. Two dot lines mark an about 65 nm wide grain boundary zone, in which the number of the precipitates is much less than the grain interior. The precipitates in the lower-left side SiC grain cannot be distinguished because of the unfavorable imaging orientation.

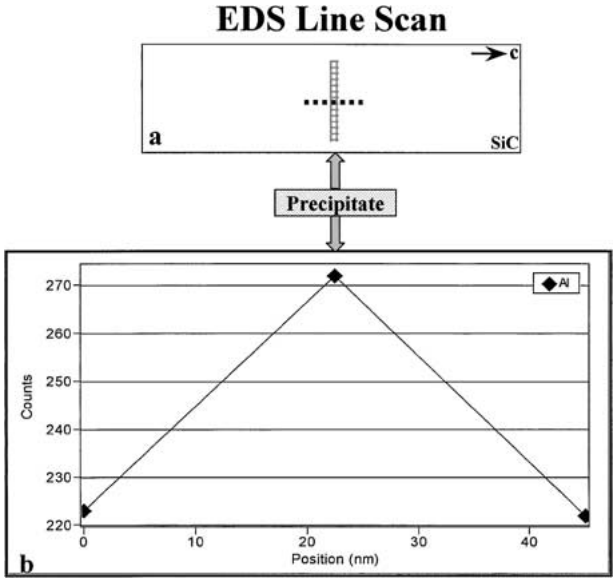

Figure 6 (a) A schematic illustration for EDS line-scan across a nano-precipitate in a SiC grain. (b) Aluminum profile along a line, which was scanned by an 8 nm diameter electron beam probe, is presented. The EDS counts are proportional to the concentration. Note the increased Al concentration at the position of the precipitate.

Al content is plotted. An Al-rich composition for the nano-precipitate was evident.

Detection of O, B, and C in the precipitates was not possible because of their weak EDS signals and, therefore, a full compositional analysis could not be made for the truly nanoscale precipitates. However, nEDS compositional analysis was possible for large precipitates in the 1600°C-annealed samples, and for large enough ones occasionally encountered in the samples annealed at 1400 or 1500°C (e.g., a 24 nm × 50 nm precipitate was observed in a 1400°C-annealed sample). nEDS spectra obtained from a precipitate and from its adjacent matrix region in the 1600°C-annealed SiC, are shown in Fig. 7a, b, respectively.

The matrix spectrum in Fig. 7b was acquired in a SiC area about 20 nm away from the precipitate under analyzed to avoid possible signal interference. Both spectra were acquired under the same experimental conditions. Therefore, Fig. 7b could serve as a background reference, which then was subtracted from the spectrum in Fig. 7a. The resulting net counts yielded a composition of $(Al_4C_3)_{1.0}\cdot(SiC)_{0.3}\cdot(B_4C)_{0.2}$. This composition can be regarded as Al_4C_3-based with minor SiC and B_4C solutions. The same nEDS quantification was obtained for precipitates in the 1400°C- and 1500°C-annealed samples. It is known that a significant alloying of Al_4C_3 with SiC or B_4C leads to structural changes, e.g. formation of Al_4SiC_4 ($Al_4C_3\cdot SiC$ [20]), or $Al_8B_4C_7$ ($2Al_4C_3\cdot B_4C$ [21]). However, no pronounced change was expected for the Al_4C_3 structure in our case because of the relatively low Si and B contents in the precipitates. This assertion was verified by high-resolution electron microscopy.

Fig. 8a shows a high-resolution image for a nanoscale precipitate in a 6H-SiC matrix grain in the 1400°C-annealed SiC. The SiC grain was imaged along the $[1\,1\,\bar{2}\,0]$ zone-axis direction. The central area of the image shows a crystalline precipitate, which is about

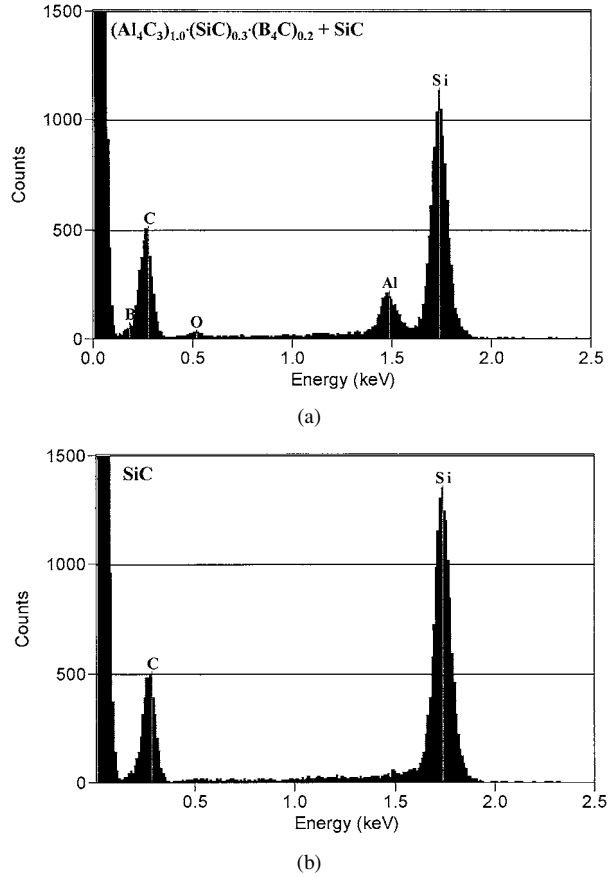

Figure 7 Point EDS spectra obtained from (a), a large precipitate in 1600°C-annealed SiC, and (b), an area in the SiC matrix 20 nm away from the precipitate under analyzing. The spectrum in (b) was subtracted from that in (a) to get net counts for the EDS peaks. An Al_4C_3-based composition was therefore determined for the precipitate, which contained B_4C and SiC solid solutions as marked in (a).

7.5 nm long, and 2.4 nm thick. A Fourier transform of Fig. 8a is presented in Fig. 8b, in which the $[1\,1\,\bar{2}\,0]$ zone-axis diffraction pattern of the 6H-SiC matrix is dominant. A (0006) reflection from the 6H-SiC is labeled and used as an internal reference to index extra reflections such as those indicated by double-headed arrows. The indicated extra reflections could be assigned since they were well separated from the SiC main reflections. Unfortunately, a halo of the multiple (000*l*) SiC reflections makes it impossible to distinguish any extra reflections along the SiC [0001] direction. Nevertheless, the visible extra reflections allowed for identification of the precipitate image as consistent with an Al_4C_3 structure projected along the $[1\,1\,\bar{2}\,0]$ direction. The indices marked in Fig. 8b support a rhombohedral structure with $a = 3.34$ Å and $c = 24.9$ Å, which precisely fit the lattice parameters for bulk Al_4C_3 with a $R\,\bar{3}\,m$ rhombohedral structure. This agreement was further confirmed by a computer-simulated electron diffraction pattern for Al_4C_3 along the $[1\,1\,\bar{2}\,0]$ zone-axis, as shown in Fig. 8c, in which the arrows indicate reflections experimentally found as the extra reflections in Fig. 8b.

Following Fig. 8, the coherent orientation relationships between the matrix α-SiC and the Al_4C_3-based precipitate were determined as:

$$(0001)_{Al_4C_3} \,//\, (0001)_{SiC},\quad [1\,1\,\bar{2}\,0]_{Al_4C_3} \,//\, [1\,1\,\bar{2}\,0]_{SiC}.$$

These orientation relationships were observed for most precipitates. The precipitates and orientation

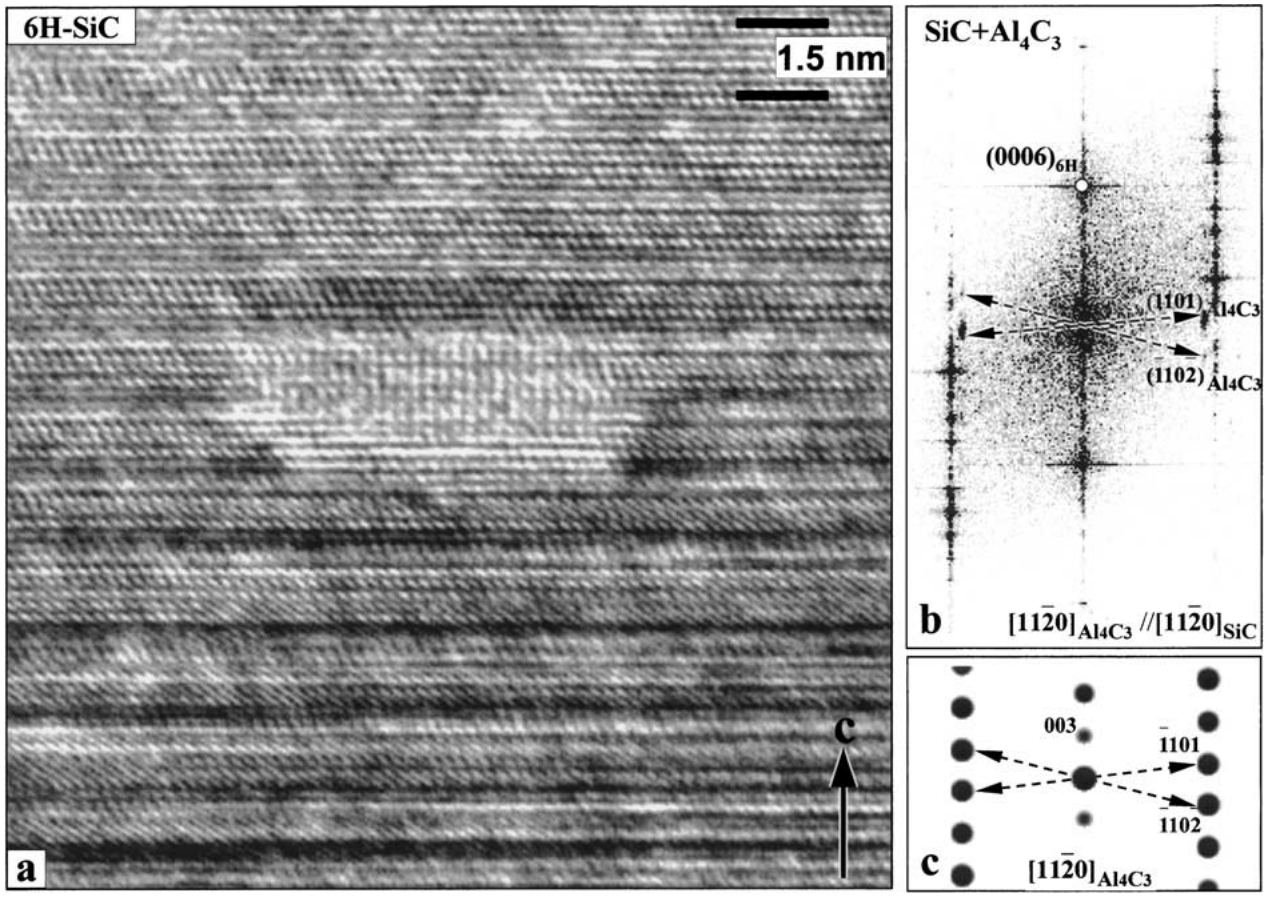

Figure 8 (a) High-resolution image showing crystalline structure of a nano-precipitate in the 6H-SiC matrix. The image was taken along the [1 1 $\bar{2}$ 0] zone-axis direction of the hexagonal SiC structure. Some buckled atomic planes can be seen in the precipitate, at a glance angle along the **c**-normal direction. (b) A Fourier transform from the high-resolution image in (a). The (0006) reflection from the α-6H SiC is marked as $(0006)_{6H}$. Extra reflections, indicated by double-head arrows, can be indexed as ($\bar{1}$ 1 0 1) and ($\bar{1}$ 1 0 $\bar{2}$), respectively, based on the Al_4C_3 [1 1 $\bar{2}$ 0] zone-axis diffraction pattern. (c) A computer simulated electron diffraction pattern for the Al_4C_3 structure along the [1 1 $\bar{2}$ 0] zone-axis direction. Double-head arrows indicate reflections experimentally observed in (b).

relationships with SiC found here are similar to those for Al_4C_3 precipitates in Al-implanted α- and β-SiC [20, 22, 23]. B_4C precipitates with a similar morphology were also reported by More *et al*. in SiC sintered with B and C additives (without Al), upon heating above 1500°C [24].

The (0001) habit planes of the precipitates were likely the result of the good lattice-matching between the precipitates and the SiC matrix. The 6H-SiC and Al_4C_3 structures projected on (0001) planes, respectively, are schematically shown in Fig. 9, in which two-dimensional unit cells are drawn.

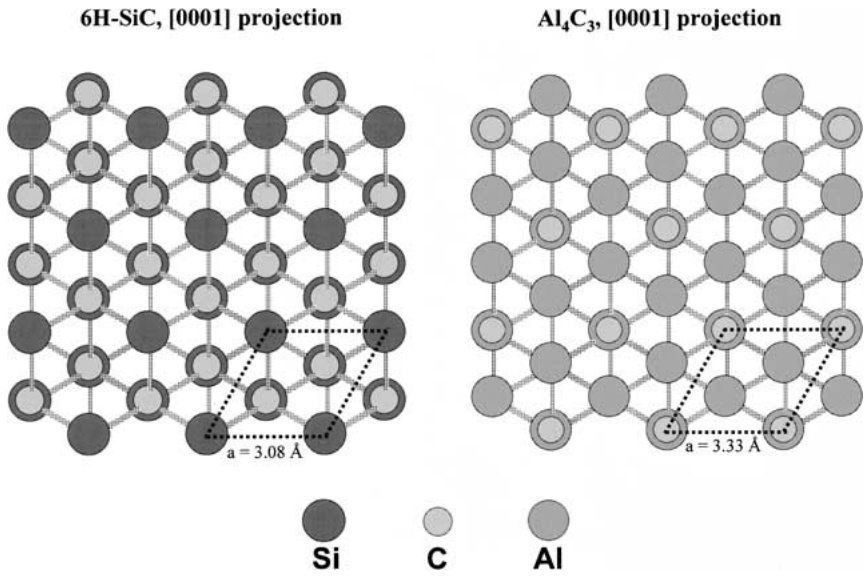

Figure 9 [0001] projected structures for the 6H-SiC and the Al_4C_3, respectively. Grey color dashed lines represent the Si-C, or Al-C bonds. Atoms on different atomic layers along the projected direction cause the visual superposition in the projection. The dot lines marked the two-dimensional unit cells for the two structures, respectively.

The two structures demonstrate high degree of coherence in lattice-matching with the preferred orientation relationships as presented. Because the lattice spacing of the bulk Al_4C_3 is about 8.1% larger than that of the bulk SiC, the compressing strain caused buckled lattice planes in the Al_4C_3 precipitates, as can be seen in Fig. 8a, at a glance angle along the **c**-normal direction. Some fine precipitates might also slightly rotate in the (0001) planes, or tilt off the SiC (0001) planes, to accommodate the lattice-mismatch strain. While the rotation in the (0001) planes resulted in a loss of point-to-point resolution in high-resolution images, the small out-plane tilting can be seen directly in Fig. 10, in which the (0001) planes of the precipitate framed by dashed lines were tilted clockwise by about 7° with respect to the SiC (0001) planes. The tilted Al_4C_3 lattice superimposes on the SiC lattice, resulting in moiré fringes. Consequently, no strain-field, nor dislocations or microcracks, were observed around the nano-precipitates. Large outplane tilting of the precipitates was also observed in 1600°C-annealed samples as have been shown in Fig. 3.

The number of the nano-precipitates counted in given areas, together with the computer-simulated foil thickness for high-resolution imaging, yields an estimate for an Al content in SiC grains. The value for the 1400°C-annealed samples was consistent with ~2 wt%, which was detected interior the SiC grains in the as-hot-pressed samples [16]. This consistency indicated that most dissolved aluminum during the hot pressing has been quantitatively precipitated after the 1400°C annealing. The nearly zero Al content in SiC grains after annealing was also confirmed by the nEDS spectra such as that in Fig. 7b, verifying the earlier assertion of quantitative precipitation.

4. Discussion

4.1. Formation of nanoscale precipitates in hot-pressed SiC

During hot pressing grain boundary phases, containing Al, B, and C, and triple-junction phases were formed [8, 16, 19]. Al, B, and C also can enter the SiC lattice [22, 25], with an increasing solubility with temperature [18]. After cooling to room temperature, the SiC bulk is essentially supersaturated with Al, B, and C. In our experiments, about 2 wt% Al was consistently detected in SiC grains in as-hot-pressed samples [16].

The subsequent heat treatments at and above 1300°C promoted atomic diffusion in the SiC lattice (Fig. 5 and text) leading to nucleation of precipitates. The growth of the nuclei was apparently diffusion controlled, as indicated by the fact that higher annealing temperatures, and thus faster diffusion rates, led to the

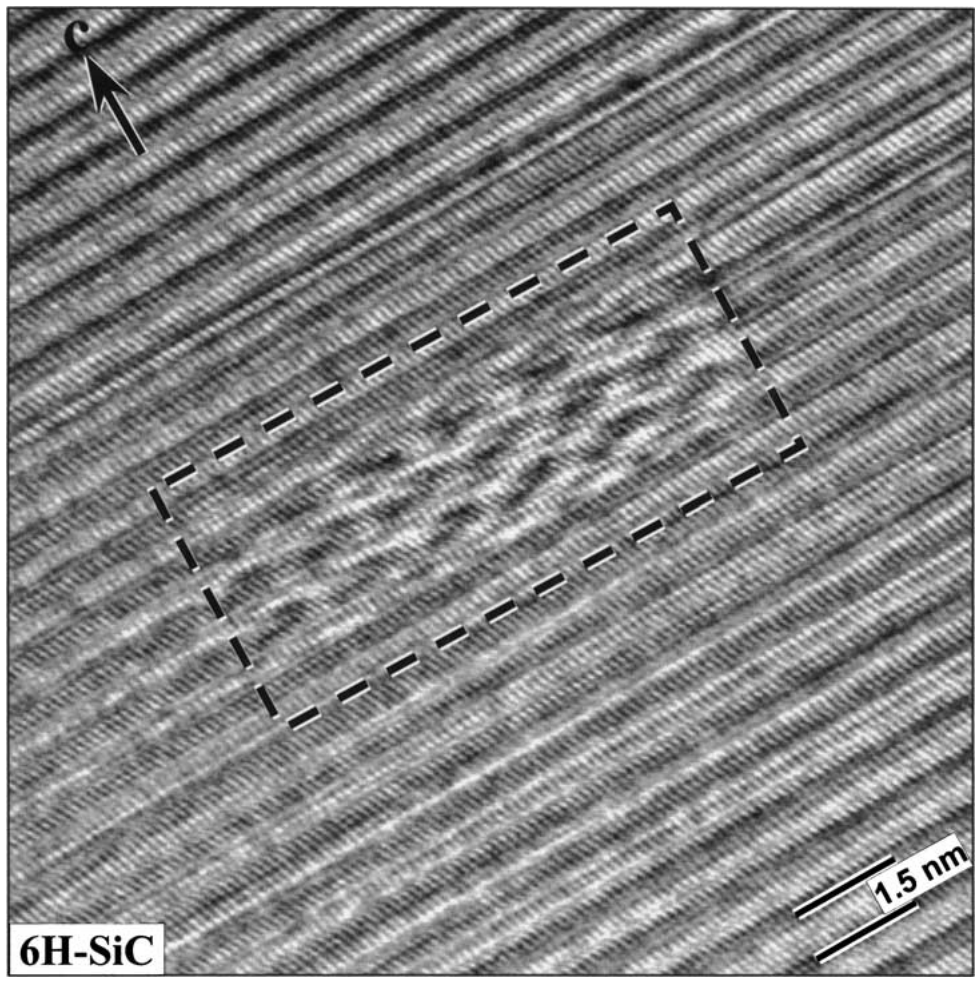

Figure 10 High-resolution image taken along the [1 1 $\bar{2}$ 0] zone-axis direction of a 6H-SiC grain. Inside the dashed-line frame is a nano-precipitate, which was not perfectly aligned with the SiC matrix. An about 7° clockwise tilting of the Al_4C_3 (0001) plane about the incident beam direction results in moiré fringes in the framed region.

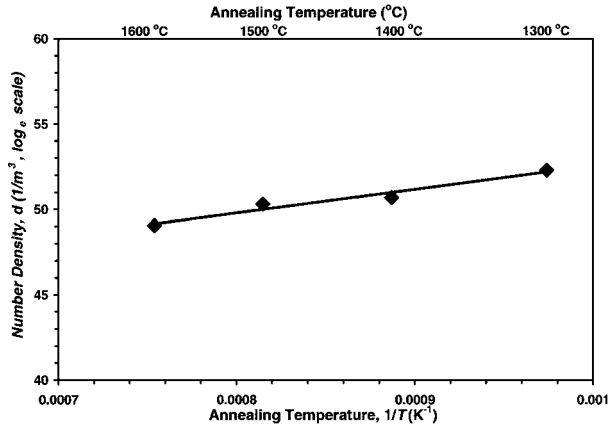

Figure 11 Change of number density of precipitates (d) as a function of annealing temperature $1/T$ (note the unit for T is Kelvin). Linear relation is seen.

larger precipitates. As a result of the nucleation and growth, Al_4C_3 precipitates, containing some Si and B were formed.

It was interesting to note that the number density of the precipitates formed between 1300 to 1600°C varied inversely with the annealing temperature (Table I). Fig. 11 shows the approximately linear relationship between ln(d), the logarithm of observed projected density, and $1/T$, consistent with classical nucleation theories.

4.2. Possible influences on mechanical properties of SiC

With the grain boundary film thickness between 0.8 to 2 nm [16], the >50 nm wide Al-depletion zones on both sides of the grain boundaries, implies a significant change of the grain boundary chemistry with annealing time. This leads one to expect significant changes in the mechanical properties of the SiC that depend sensitively on grain boundary properties. Such changes were observed. For example, our study showed a recovery of high temperature strength and toughness of the ABC-SiC upon annealing time, Fig. 12. Although the amorphous grain boundary films were found crystallized during the annealing [16], the strength recovery rates were considerably slower than the rates of grain boundary crystallization. It may thus reasonably be postulated that the slow improvement of these high temperature mechanical properties are intimately related to gradual Al enrichment of the grain boundary films.

Although it is unlikely that the nano-precipitates reported here would affect bulk long-crack fracture toughness, their high density and uniformly dispersion could enhance the in-grain microcrack toughness. Therefore, for mechanical properties that depend on microcrack initiation, such as abrasive wear and impact erosion, the in-grain toughening may have a positive influence. A change in wear resistance of the ABC-SiC after appropriate post-annealing was indeed observed [26]. Furthermore, the precipitates could also play a role in reducing creep at temperatures higher than 1600°C where dislocation motion becomes important [27–29].

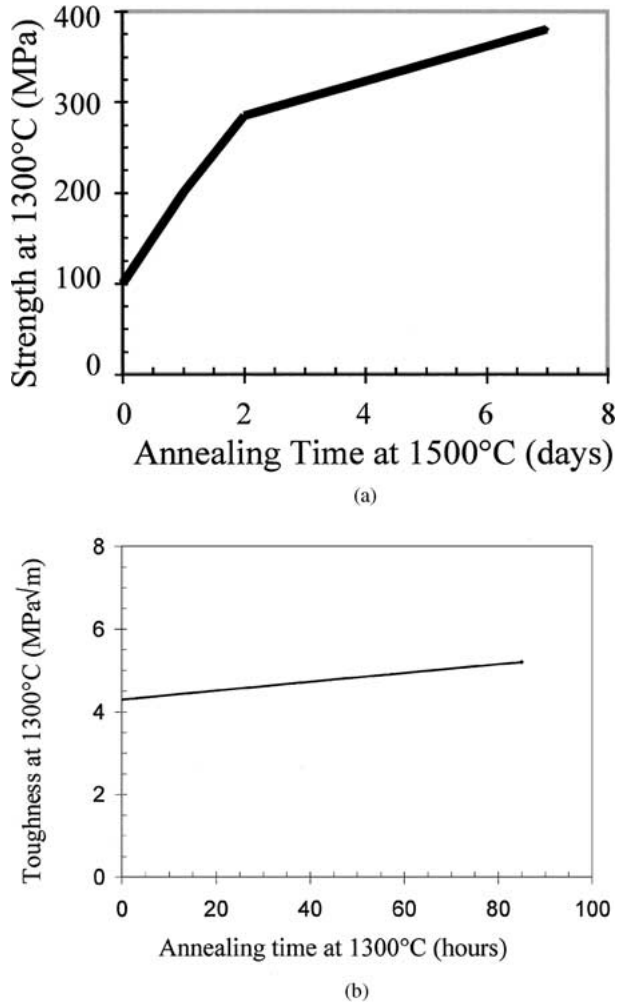

Figure 12 Gradual recovery of (a), bend strength and (b), toughness, at 1300°C as a function of annealing time.

5. Summary

Highly dense and uniformly dispersed nano-precipitates were produced in ABC-SiC by heat treatment at 1300°C, 1400°C, 1500°C, and 1600°C in Ar. The precipitates coarsened while the number density decreased with increasing annealing temperature. TEM identified the coherent Al_4C_3-based precipitate structure, while nEDS confirmed the Al_4C_3-based composition containing minor amounts of Si and B. At 1400°C, precipitation of Al was quantitative, whereas no precipitation occurred at 1200°C even after long time annealing, most likely due to slow diffusion kinetics. The preferred orientation relationship between the precipitates and the matrix was determined. Grain boundaries were surrounded by depleted zones, which allowed for an estimate of the Al diffusion coefficient in SiC at elevated temperatures, and of the Al concentration increase in the grain boundary films. The slow but substantial increase in Al content of the grain boundary films was correlated with a gradual improvement in mechanical properties of the ABC-SiC upon extended annealing at high temperatures. Formation of the nanoscale precipitates followed classical nucleation concepts. The uniformly dispersed fine precipitates in the SiC grains were thought to be of potential benefit to mechanical properties that are determined by microcrack initiation.

Acknowledgment

This work was supported by the Director, Office of Energy Research, Office of Basic Energy Sciences, Materials Sciences Division of the U.S. Department of Energy under Contract No. DE-AC03-76SF0098. Part of this work was made possible through the use of the National Center for Electron Microscopy facility at the Lawrence Berkeley National Laboratory.

References

1. R. W. RICE, S. W. FREIMAN and P. F. BECHER, *J. Amer. Ceram. Soc.* **64** (1981) 345.
2. R. W. RICE and S. W. FREIMAN, *ibid.* **64** (1981) 350.
3. W. R. CANNON and T. G. LANGDON, *J. Mater. Sci.* **18** (1983) 1.
4. R. H. DAUSKARDT, W. YU and R. O. RITCHIE, *J. Amer. Ceram. Soc.* **70** (1987) C-248.
5. S. W. FREIMAN, *Ceramic Bulletin* **67** (1988) 392.
6. H. J. KLEEBE, M. K. CINIBULK, R. M. CANNON and M. RÜHLE, *J. Amer. Ceram. Soc.* **76** (1993) 1969.
7. S. M. WIEDERHORN, B. J. HOCKEY, D. C. CRANMER and R. YECKLEY, *J. Mater. Sci.* **28** (1993) 445.
8. J. J. CAO, W. J. MOBERLYCHAN, L. C. DE JONGHE, C. J. GILBERT and R. O. RITCHIE, *J. Amer. Ceram. Soc.* **79** (1996) 461.
9. C. J. GILBERT, J. J. CAO, L. C. DE JONGHE and R. O. RITCHIE, *ibid.* **80** (1997) 2253.
10. Q. JIN, X. G. NING, D. S. WILKINSON and G. C. WEATHERLY, *ibid.* **80** (1997) 685.
11. W. J. MOBERLY, CHAN, J. J. CAO and L. C. DE JONGHE, *Acta Materialia* **46** (1998) 1625.
12. D. CHEN, C. J. GILBERT, X. F. ZHANG and R. O. RITCHIE, *ibid.* **48** (2000) 659.
13. D. CHEN, X. F. ZHANG and R. O. RITCHIE, *J. Amer. Ceram. Soc.* **83** (2000) 2079.
14. Y. M. CHIANG, L. A. SILVERMAN, R. H. FRENCH and R. M. CANNON, *ibid.* **77** (1994) 1143.
15. Q. JIN, D. S. WILKINSON and G. C. WEATHERLY, *ibid.* **82** (1999) 1492.
16. X. F. ZHANG, M. E. SIXTA and L. C. DE JONGHE, *ibid.* **83** (2000) 2813.
17. M. E. SIXTA, X. F. ZHANG and L. C. DE JONGHE, *ibid.* in press.
18. Y. TAJIMA and W. D. KINGERY, *Communications of the American Ceramic Society* (1982) C27.
19. X. F. ZHANG, M. E. SIXTA and L. C. DE JONGHE, *J. Amer. Ceram. Soc.* **84** (2001) 813.
20. L. L. ODEN and R. A. MCCUNE, *Metallurgical Transactions A* **18A** (1987) 2005.
21. Z. INOUE, H. TANAKA and Y. INOMATA, *J. Mater. Sci.* **15** (1980) 3036.
22. H. H. DU, Z. YANG, M. LIBERA, D. C. JACOBSON, Y. C. WANG and R. F. DAVIS, *J. Amer. Ceram. Soc.* **76** (1993) 330.
23. J. STOEMENOS, B. PÉCZ and V. HEERA, *Appl. Phys. Lett.* **74** (1999) 2602.
24. K. L. MORE, C. H. CARTER, JR., J. BENTLEY, W. H. WADLIN, L. LAVANIER and R. F. DAVIS, *J. Amer. Ceram. Soc.* **69** (1986) 695.
25. W. J. CHOYKE and G. PENSL, *MRS Bulletin* (1997) 25.
26. X. F. ZHANG, D. CHEN, Q. YANG, G. LEE, R. O. RITCHIE and L. C. DE JONGHE, to be submitted.
27. J. E. LANE, C. H. CARTER and R. F. DAVIS, *J. Amer. Ceram. Soc.* **71** (1988) 281.
28. R. D. NIXON and R. F. DAVIS, *ibid.* **75** (1992) 1786.
29. G. S. CORMAN, *ibid.* **75** (1992) 3421.

Received 1 August 2000
and accepted 3 August 2001